Electron reflection and interference in the GaAs/AlAs-Al Schottky collector resonant-tunneling diode

A. J. North,* E. H. Linfield, M. Y. Simmons, and D. A. Ritchie
Cavendish Laboratory, University of Cambridge, Cambridge CB3 0HE, United Kingdom

M. L. Leadbeater, J. H. Burroughes, and C. L. Foden
Toshiba Cambridge Research Centre, 260 Cambridge Science Park, Cambridge CB4 4WE, United Kingdom

M. Pepper
Cavendish Laboratory, University of Cambridge, Cambridge CB3 0HE, United Kingdom
and Toshiba Cambridge Research Centre, 260 Cambridge Science Park, Cambridge CB4 4WE, United Kingdom

(Received 11 July 1997)

Schottky collector resonant-tunneling diodes (SCRTD's) have potential for increased oscillator bandwidth, but may be prone to electron reflection at the semiconductor-metal interface of the Schottky collector. This reflection has been observed previously using collectors deposited *in situ* by molecular beam epitaxy: the reflection was manifested as interference oscillations on the rising slope of the resonant current. This paper extends the room temperature results of that work to cover the 1.5 K–300 K range, revealing valuable information on the semiconductor-metal interface, scattering rates, scattering mechanisms, peak-to-valley ratios, electron distribution, and electron transport. The SCRTD oscillation strength was found to depend on the above-barrier reflection coefficient of the collector metal, and the effect of scattering on virtual states confined by this reflection. Increased scattering degrades the oscillation strength as temperature is increased. The primary scattering mechanism was determined to be LO phonon emission, which had a related role in degrading the main peak-to-valley ratio through scattering in the well of the resonant-tunneling diode (RTD). The number of oscillations was dependent on the emitter electron distribution, with thermally activated oscillations appearing at high temperature. Increasing temperature caused a voltage shift of the oscillations that followed the GaAs band-gap temperature dependence, implying pinning relative to the GaAs valence band and interface states with valence-band wave functions. Postresonant oscillations were thought to arise from transport through the transverse X valley of the second AlAs RTD barrier. An Airy function model of device transmission and current is presented. [S0163-1829(97)00247-6]

I. INTRODUCTION

Double barrier resonant-tunneling diodes (RTD's) are currently the widest bandwidth semiconductor devices with gain.[1] When an RTD is suitably biased in a tuned circuit, gain is provided by the device's negative differential resistance (NDR), allowing sustained oscillation. In 1989 Brown and co-workers used a small signal RTD equivalent model to examine the role of intrinsic device parameters in determining $f_{\max}$, the frequency limit of gain.[2,3] The equations presented predict a higher $f_{\max}$ in designs with reduced parasitic impedances L, C, and R_s. The inductance L was said to be proportional to the well-state lifetime, the limiting factor of switching speed. L is reduced by using thin barriers, allowing a simultaneous increase in conductance and oscillation power. Heavy emitter doping further increases supplied power. The emitter-collector capacitance C is reduced using an undoped spacer separating the collector and double barrier. Larger spacer widths give decreased capacitance, but lead to long electron transit times and decreased NDR through voltage-length scaling of the I-V characteristic. It is possible to avoid this trade-off by moving from traditional GaAs/AlAs RTD's to InAs/AlSb RTD's,[4] where the transit velocity is higher and the indium specific contact resistance is lower: the reduced series resistance R_s gives a smaller time constant R_sC. Another route to reduced time constant has been suggested by Konishi *et al.*[5] and Smith *et al.*,[6] using a Schottky collector in place of the normal Ohmic contact. The Schottky presents zero small signal impedance, allowing a large reduction in R_s at the cost of increased device bias. Using an aluminum collector, a 17 Å/45 Å/17 Å AlAs/GaAs/AlAs RTD and a 350-Å spacer, they named the structure the Schottky collector RTD (SCRTD).

Konishi *et al.*[5] mentioned the possibility of electron reflection at the aluminum interface, though their results gave no evidence for this. In contrast, Weckworth, van der Wagt, and Harris[7] observed oscillations on the rising slope of the RTD current in a similar device, but with *in situ* deposited aluminum. The oscillations were attributed to quantization in the collector spacer, caused by the finite above-barrier reflection coefficient of the Schottky barrier biased beyond flat band. The clarity of the effect is apparently related to the uniformity of the GaAs-Al interface, enhanced in Ref. 7 by the *in situ* deposition. Reflection at epilayer interfaces and the resulting interference has since been reported elsewhere in normal Ohmic contacted thin barrier RTD's.[8] The results in this paper explore the effect of variable temperature on *in situ* fabricated SCRTD's.

 © 1998 The American Physical Society

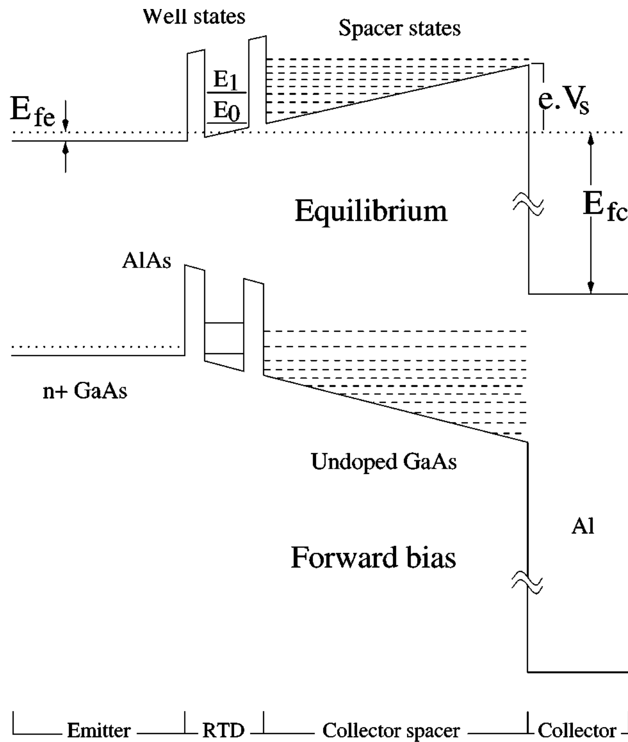

FIG. 1. Schematic equilibrium and forward bias band diagrams for a SCRTD, showing well states (solid) and spacer states (dashed). The well ground state in the biased diagram (E_0) lies between the emitter Fermi energy E_{fe} and the conduction-band edge, allowing resonant tunneling into the spacer. In the diagram, though, E_0 lies between quasibound spacer states, so a minimum in conductance would be expected. eV_s is the Schottky barrier height ($\sim$0.8 eV) and E_{fc} is the Fermi energy of the aluminum collector ($\sim$11.6 eV).

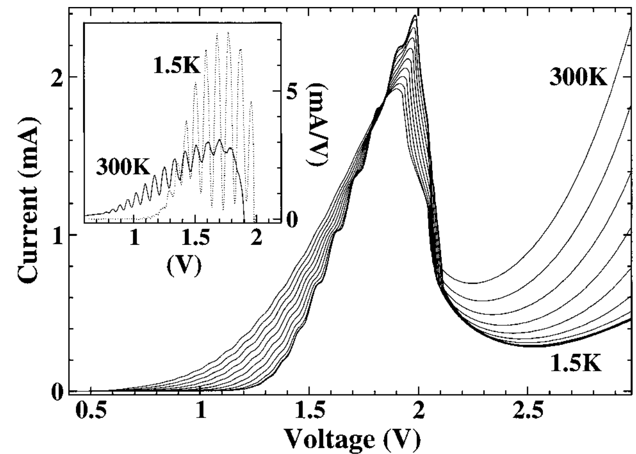

FIG. 2. C763 SCRTD I-V curves, measured at 1.5 K, and every 30 K from 30 K to 300 K. The oscillations on the rising slope of the resonant characteristic are seen more clearly in the inset of differential conductance. dI/dV is shown at 1.5 K and 300 K.

II. FABRICATION

Three wafers were grown on (100) GaAs substrates for this study. Wafers C763 and C767 were grown with 20 Å/50 Å/20 Å AlAs/GaAs/AlAs structures in a VG V80H MBE machine, with undoped collector spacers of 550 Å and 300 Å, respectively. The $C(V)$ measured emitter doping levels were 2.2×10^{18} cm^{-3} and 1.9×10^{18} cm^{-3}, the silicon dopant being incorporated in half micron layers, separated from the RTD's by a 100-Å undoped layer. T203 was grown in a Varian Gen II with 30 Å barriers and a 250-Å collector spacer. Its emitter comprised (in growth order) a 2000-Å 10^{18} cm^{-3} doped layer, a 500-Å layer with doping graded to 10^{17} cm^{-3}, and a 200-Å undoped layer. Each growth included a 15-h growth interrupt during which the arsenic overpressure was pumped away. Aluminum deposition of 2000-Å layers commenced the next day at a substrate temperature of ~-14 °C, and a chamber pressure of $\sim1.5\times10^{-9}$ Torr. The rate used was 0.3 μm/h, for which predominantly single-crystal material might be deduced from the results in Ref. 9. Band diagrams for the SCRTD structure are shown in Fig. 1. The bias required for tunneling through the second well state shown could not be reached (excessive current damaged the devices). Further mention of well states or resonance hence refers to the ground state of the well.

Fabrication was undertaken with the aim of cryogenically measuring stable I-V curves. With thin barriers and large current densities this required small (5 μm^2) mesas defined by electron-beam-lithography (EBL). Extrinsic voltage drops were eliminated using four-terminal contacts connected in a planar geometry with cross-linked PMMA (polymethylmethacrylate) isolation and EBL-defined contact vias.[10] The aluminum was wet etched (prior to self-aligned reactive ion etching of device mesas) using Shipley Microposit MF319 optical developer, containing tetramethylammonium hydroxide. This was determined to have an Al etch rate of $\sim$120 Å/min, and a negligible GaAs etch rate. The technique gave far superior results to dilute NaOH etching, and required no nitrogen bubbling[11] to avoid attack of the underlying GaAs. NiGeAu annealed at 380 °C was used to make contact to the emitters.

III. RESULTS

Figure 2 shows results for C763, measured with a 410 Ω parallel resistor for circuit stabilization in the NDR region beyond the resonant peak.[12] At 1.5 K there are nine oscillations on the rising slope of the resonance, corresponding to the alignment of nine spacer states with the well state while the latter is on resonance. A simple length scaling of field explains the slow shift of the well state relative to the spacer states: this is demonstrated in Fig. 1. The calculated flat band energy of the well state ($E_0=107$ meV) exceeds the low-temperature emitter Fermi energy ($E_{\mathrm{fe}}=91$ meV for 2.2×10^{18} cm^{-3} donor density), so resonant threshold occurs beyond flat band. The observed spacer states are therefore *virtual*—contained by above-barrier reflection at the metal interface. The reflection is caused by the large change in potential energy $[eV_s+E_{\mathrm{fc}}\approx(0.8+11.6)$ eV$]$ and effective mass ($m^*/m_e=0.067\rightarrow m^*/m_e=1$) experienced by electrons entering the aluminum.[7]

At high temperature the inset of Fig. 2 shows five additional oscillations at low voltage. These result from thermal smearing of the emitter electron distribution. A high-energy tail of electrons activated above E_{fe} extends the resonance to lower voltage, allowing observation of spacer states with lower quantum number. At low temperature these states cannot be probed, since they sweep past the well state before the

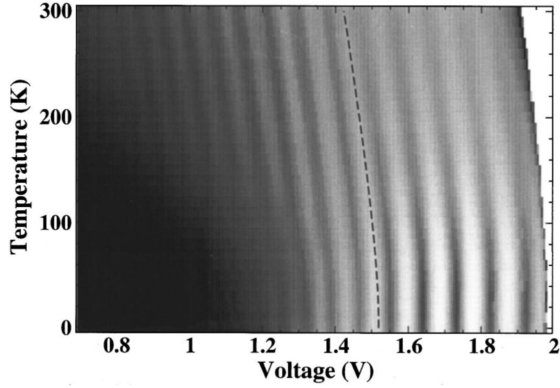

FIG. 3. Grayscale plot of the C763 temperature data, using log scale conductance data measured at 1.5 K, and every 10 K from 10 K to 300 K. The dark stripes are the conductance minima following each oscillation.

onset of emitter→well tunneling. The thermal smearing can be modeled using the coherent current formula from Ref. 13, modified to account for the rectifying Schottky barrier. For a device of area A, transmission probability $T(E_\perp)$ and three-dimensional (3D) emitter density of states, the device current is

$$I=\int_0^\infty T(E_\perp)S(E_\perp)dE_\perp ,$$

$$\text{where}\quad S(E_\perp)=\frac{Aem^*kT}{2\pi^2\hbar^3}\ln\left[1+\exp\left(\frac{E_{\rm fe}-E_\perp}{kT}\right)\right] \qquad (1)$$

is the emitter supply function. $E_\perp$ is the component of emitter electron energy perpendicular to the barriers. The temperature dependence of $S(E_\perp)$ can easily be shown to reproduce the background of the C763 characteristics, using a fixed area δ-like transmission profile $T(E_\perp)$ and simple linear scaling of well-state energy with voltage. To reproduce the current oscillations the integrated transmission $\int T(E_\perp)dE_\perp$ must oscillate as a function of $E_\perp$ and voltage. Computer modeling shows this occurs due to an oscillation of transmission linewidth, or, equivalently, tunnel broadening of the well state by alignment with spacers states. The amplitude of the oscillation depends on the aluminum reflection coefficient, which determines the strength of standing wave interference in the spacer, and consequent modulation of its density of states.

Examination of Fig. 2 shows a shift of the I-V curves to lower bias with increasing temperature. The shift is shown more clearly by tracing oscillation position in the grayscale of Fig. 3, a log function of conductance. The cause of the shift is the temperature dependence of the built-in potential or flat band voltage $V_{\rm bi}$, which represents an additive voltage offset of the I-V curves. Figure 1 shows $V_{\rm bi}$ to depend on two temperature-dependent parameters: the emitter Fermi energy and Schottky barrier height, with $V_{\rm bi}=E_{\rm fe}/e+V_{\rm s}$. The temperature dependence of $E_{\rm fe}/e$ was calculated to be small relative to the observed 0.1 V shift, varying less than 6 mV over the 300-K range. The other component $V_{\rm s}$ varies as some function of the GaAs band-gap temperature dependence and metal Fermi-energy pinning position. The band-gap temperature dependence is given in Ref. 14 as $E_{\rm g}=[1.519-5.405\times10^{-4}\ T^2/(T+204)]$ eV, which, converted to voltage as $E_{\rm g}/e$, is plotted in Fig. 3 as the dashed line. The line is seen to follow the oscillations. If the change in $E_{\rm fe}/e$ is neglected, this implies $V_{\rm s}$ changes in the same manner as $E_{\rm g}/e$, with the metal Fermi energy pinned relative to the GaAs valence band. This tends to support a conclusion drawn in a study of epitaxial silicide-silicon diodes,[15] which stated that the semiconductor contribution to the interface states that pin the Fermi energy of a metal-semiconductor junction is dominated entirely by the nearest semiconductor band. In this case the result implies the interface states have valence-band wave functions. Note we have assumed here that the four-terminal measurement eliminates contact resistance and gives band diagram energy shifts corresponding to the applied bias.

Another aspect of interest in the grayscale is the oscillation strength, which as a function of voltage is a balance of two competing processes. Increased spacer-state quantum number implies an increased well-state alignment voltage and larger above-barrier energy for electrons impinging on the aluminum. Since the above-barrier reflection coefficient decreases monotonically with energy the interference caused by the reflected waves decreases, progressively weakening the oscillation strength. Countering this effect on the current integral of Eq. (1) is a supply function that increases with voltage (the well state and tunneling electron energy $E_\perp$ drop in energy with increasing bias). The increase in supply function amplifies the current modulation. Modeling incorporating the two effects shows the low-temperature oscillation strength to be maximized midrange at $\sim$1.7 V, agreeing with the grayscale (the conductance minima are darkest here).

As a function of temperature the oscillation strength shows two regimes. Below $\sim$1.4 V it increases with increasing temperature, while at higher voltage, it decreases. This again results from a balance of two competing processes. In the low-voltage regime the well state lies near the emitter Fermi energy; Fig. 2 shows the two align at $\sim$1.2 V, the low-temperature threshold. The tunneling electrons at biases near this voltage have energies $E_\perp$ near the Fermi energy, where the temperature dependence of the supply function is strongest. The increase of $S(E_\perp)$ with increasing temperature amplifies the current modulation. In the high-voltage regime the well state lies further down in energy, where the supply function increases much more slowly with temperature. Temperate-dependent scattering processes dominate here, causing a decrease in oscillation strength with increasing temperature.

Possible candidates for the scattering mechanisms were nominated by comparing scattering times with calculated dwell times. At 1.4 V the spacer transit time is $\tau_{\rm trans}=67$ fs, calculated using the semiclassical equations of motion and an effective two-level nonparabolic dispersion relation $\hbar^2k^2/2m^*=E(1+E/E_0^*)$, with $E_0^*=1$ eV chosen for the [100] direction.[16] The transit time decreases to 57 fs at 2 V—a small change implying a near saturated velocity (10^8 cm/s),[16] caused by band nonparabolicity rather than mobility limited saturation. The spacer dwell time is calculated by neglecting escape back into the well (resonant tunneling into the emitter is highly unlikely, since beyond 1.4 V the emitter states are almost fully occupied at the tunneling

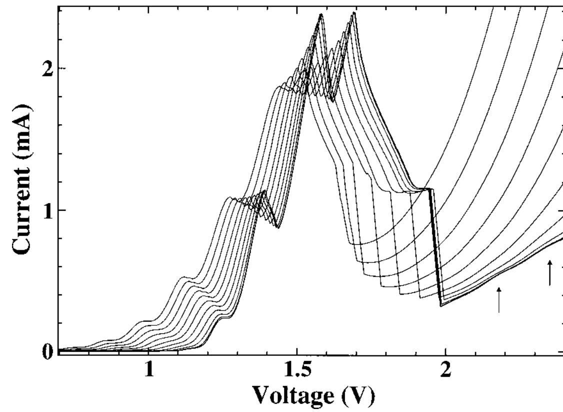

FIG. 4. C767 SCRTD I-V curves, measured at 1.5 K, and every 30 K from 30 K to 300 K.

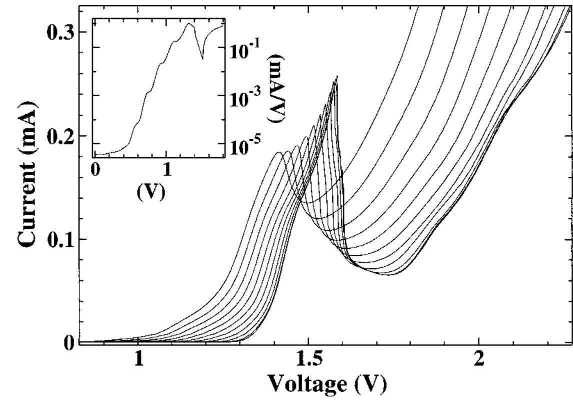

FIG. 5. T203 SCRTD I-V curves, measured at 1.5 K, and every 30 K from 30 K to 300 K. The 300 K conductance is shown inset, with weak oscillations in the thermally activated current.

energy). If transmission from the spacer into the aluminum is labeled by T_{sa}, a summation of multiple-reflection probability-weighted times leads to a geometric progression and spacer dwell time $\tau_s = \tau_{trans} T_{sa}/(2T_{sa}-1)$. Calculated values for T_{sa} are over 0.96 above 1.4 V, so the dwell time is on average not much greater than the transit time, and most electrons will make just one transit. Of course these electrons are not responsible for the interference, and scattering will degrade oscillation strength by phase randomization of electrons making multiple transits. It is clear, however, that scattering is much more likely in the quantum well, since this has a much longer dwell time of $\tau_w = 5$ ps (calculated using the transmission linewidth of a coherent model[17]). LO phonon and electron-electron scattering are both likely to have time scales smaller this, and are suitable candidates for analysis of our data.

To clarify the effect of scattering, we first present data for the other two wafers. The temperature dependence of C767 is shown in Fig. 4. Stabilizing resistors were not used, so the curves show a plateau in the NDR region, representing a dc average of unstable oscillation. The resonance width is smaller than C763's, partly due to the reduced emitter Fermi energy (82 meV at 1.5 K), but mostly due to the reduced spacer thickness, which causes the well state to move down in energy more quickly with bias. The thermal activation and band-gap shift are again apparent, and the curves show fewer, more widely spaced oscillations, as expected from the confinement energies of the thinner spacer. The oscillations are much stronger in this device, suggesting either an enhanced aluminum reflection coefficient or reduced scattering. Interfacial contamination representing a *real* barrier for electrons impinging on the aluminum could dramatically enhance the reflection coefficient, but was not thought likely given the high-vacuum growth conditions. Since the growth conditions were identical for C763 and C767, we take this to imply that scattering in the spacer plays a major role in oscillation strength, with the decreased transit time of C767 leading to a reduced scattering probability. At 1.4 V the calculated C767 transit time is 36 fs, from which we infer a scattering time scale of the same order.

The two arrows in Fig. 4 point to postresonant oscillations. Like the on-resonance oscillations, these probably result from real-space electron transfer between 2D states, but they do not shift in voltage when a magnetic field is applied perpendicular to the current direction. This implies that the transfer does not conserve momentum.[8,18] An obvious possibility here is LO phonon emission-assisted transfer from 2D emitter states to the post-resonant well state. An emitter accumulation layer is not thought to exist in this sample, however, given the high dopant density near the RTD and broad resonant peak, which indicates a 3D emitter density of states. If the oscillations *were* caused by phonon emission from an emitter accumulation layer, they would split in magnetic field applied parallel to the current direction, due to Landau-level quantization.[19] No splitting was observed up to 9 T. Furthermore, in a separate experiment with a stabilizing resistor and 2.7 V bias range, many post-resonant oscillations were revealed. High-order LO phonon processes are unlikely, and the features had the same voltage spacing as the on-resonance oscillations, implying spacer-state involvement. The mechanism responsible is thought to involve a momentum nonconserving probing of the spacer density of states by states confined to the transverse X valleys of the second AlAs barrier.

Figure 5 shows the T203 temperature dependence. The reduced current of this thicker barrier device allowed capacitive[20] stabilization of the NDR characteristic, with a 50 Ω-6 μF series RC circuit connected in parallel to the RTD. The T203 results are markedly different from C767's, for a comparable spacer length. The oscillations are much weaker, being only just visible in the log of conductance at 300 K. There are two possible reasons for this, the first being a modified supply function. In contrast to C767 and C763, magneto-oscillations in current were detected in T203 at 1.5 K near threshold, in $0 \rightarrow 9$ T parallel magnetic field, at currents up to a maximum of 40 μA. These are caused by the depopulation of emitter Landau levels passing through the emitter Fermi energy with increasing field.[21] They require a thermalized emitter accumulation layer, provided in this sample by the reduced emitter doping and thicker emitter spacer layer. Electrons injected from the emitter contact thermalize from 3D states into the 2D accumulation layer by acoustic-phonon emission, and escape by tunneling into the well. For currents above 40 μA, the escape rate was calculated to be faster than the thermalization rate $\sim[100 \text{ ps}]^{-1}$, so the accumulation layer could not be maintained, explaining the disappearance of the magneto-oscillations. Beyond threshold (at currents above 40 μA) the form of the supply function is speculative. We think that an acoustic-phonon

bottleneck is inconsistent with the rapidly increasing current, and hypothesize a transformation of the emitter density of states from 2D to 3D, resulting from an inability of the emitter accumulation layer to screen further increases in voltage. With reduced screening, the bump in the conduction band caused by electron diffusion into the low doped emitter layers[22] would be pulled down by bias. The accumulation layer lying between the RTD and this bump would lose its confinement, and the emitter would become 3D. In any case it is clear that the form of the supply function does not follow Eq. (1), making a comparison with C767 difficult. The resonance is much thinner in T203, with room for only one on-resonance oscillation. Note again the appearance of postresonant oscillations.

The other possible cause for weakened oscillations in T203 is the increased barrier thickness. The calculated well lifetime with 30-Å barriers is 200 ps—very much longer than the 5-ps figure of the other devices. Note here that electrons must tunnel into the spacer from the well state in order to observe the oscillations, since the well state is used to probe the spacer states.[7] Inelastic transport mechanisms with time scales less than 200 ps may violate this condition, allowing escape into the spacer through scattering. This could involve (for example) phonon-assisted transfer through the X valley of the *second* AlAs barrier. This type of transport would wash out the oscillations. The postresonant data supports this idea. Stabilization of the 1.5-K C767 characteristic gives a peak-to-valley ratio (PVR) of 8.2, over two times higher than T203's value of 3.9. The poor T203 PVR may be taken to indicate a decreased coherent current component, and, in particular, increased inelastic *barrier* transfer. Broadening of the well state by scattering[23] within the well is not thought an appropriate explanation; this should not be much greater in T203 and would not be so large as to wash out the oscillations, since the spacer states have a separation of ~ 120 meV in this sample.

A comparison of results for the three wafers highlights the conditions required for maximizing oscillation visibility. Short spacers increase oscillation strength through decreased scattering. Thin RTD barriers drop the well lifetime and increase the likelihood of a coherent well$\rightarrow$spacer escape process. The reduction in inelastic escape increases oscillation strength. Heavy emitter doping gives a 3D density of states with a large Fermi energy, giving an increased resonance width—allowing the well state to probe more spacer states for a given spacer-state separation. These conditions are exactly those used for the design of Konishi and Smith's high-speed SCRTD's. The absence of oscillations in their data suggests the interface of their *ex situ* deposited aluminum is spatially nonuniform, and does not give the specular reflection required for spacer-state quantization.

Having discussed each wafer, we now pinpoint the relevant scattering mechanisms. To do this we compare the temperature dependence of possible scattering mechanisms with experimental data. Considering first the well region, we discuss the PVR of the main resonance. More specifically, we discuss its temperature dependence; in contrast to the argument of barrier transfer, the absolute value of the PVR is not important here. Using the model of Büttiker,[23] we consider the PVR to depend on scattering induced broadening of the well state, which, with temperature-dependent scatter mechanisms, leads to a temperature-dependent PVR. Thermally activated transport through the X valley of the *first* AlAs barrier leads to another source of temperature dependent postresonant current, but the energy of the X valley state is quite high,[24] and this mechanism does not contribute significantly to the temperature dependence of the valley current in these samples.

As mentioned earlier, electron-electron scattering and LO phonon scattering are likely to have time scales less than 5 ps, and with well lifetimes of 5 ps (C763,C767) and 200 ps (T203), are likely to occur in the well. In C763 and C767 electron-electron scattering can be discounted as the cause of the PVR temperature dependence, since the well electron distribution is hot, having insufficient time for acoustic-phonon thermalization. The current continuity equation $\sigma = j\tau_w/e$ (with current density j and well charge density σ) can be used with the 2D density of states $D(E)=m^*/\pi\hbar^2$ to show almost all in-plane well states are unoccupied, so the phase space available for electron-electron scattering is already large at low temperature, and does not require thermal smearing of the distribution to conform with the exclusion principle. The $\sim kT$ temperature enhancement of the phase space is relatively weak, and cannot explain the decrease in PVR. LO phonon scattering is a more likely explanation: when allowed by energy conservation, intrasubband LO phonon emission was determined to be the fastest scattering mechanism of all impurity-, defect-, and phonon-related processes considered in the quantum well of Ref. 25; this included intersubband and interwell processes.

To consider the effect of the energy-conservation requirement, note that the onset of NDR is determined by the bias at which the well state aligns with the emitter conduction-band edge. Electrons tunneling into the well at the resonant peak will therefore have a spread of in-plane energy matching the emitter energy distribution. The maximum in-plane energy of the distribution exceeds the GaAs LO phonon energy ($\hbar\omega_{LO}=36$ meV) in C763 and C767 even at low temperature, where E_{fe} is 91 meV and 82 meV, respectively. As mentioned, the emitter energy distribution of T203 is complicated, but it probably also spans a range larger than $\hbar\omega_{LO}$. With a scantly occupied or highly nondegenerate well, the energy conservation requirement for the occurrence of LO phonon emission at or beyond the current peak is satisfied.

Numerical calculation of the LO phonon scattering rate was made using formulas from Ref. 26, derived for the interaction of bulk GaAs phonons with a *single* electron confined in a quantum well. The limit of nondegeneracy was thus taken—a simplifying approximation that eliminates Fermi occupancy and screening factors. To further simplify matters, the in-plane electron energy was taken to be $\hbar\omega_{LO}$, the emission threshold. The scattering rate was then given by

$$\tau_{LO}^{-1}=\alpha\omega_{LO}[\pi(1+n_B)f(\gamma)+\sqrt{2}n_B K(1/\sqrt{2})f(\sqrt{2}\gamma)], \tag{2}$$

where $\gamma=\sqrt{2m^*\hbar\omega_{LO}}$ is the electron wave vector and $n_B = (e^{\hbar\omega_{LO}/kT}-1)^{-1}$ is the Boltzmann distribution of phonons. K, α, and f are factors defined in Ref. 25, given here by[27] $\alpha=0.07$, $K(1/\sqrt{2})=1.85$, $f(\gamma)=0.48$ and $f(\sqrt{2}\gamma) = 0.29$. The first term in the brackets of Eq. (2) is due to LO

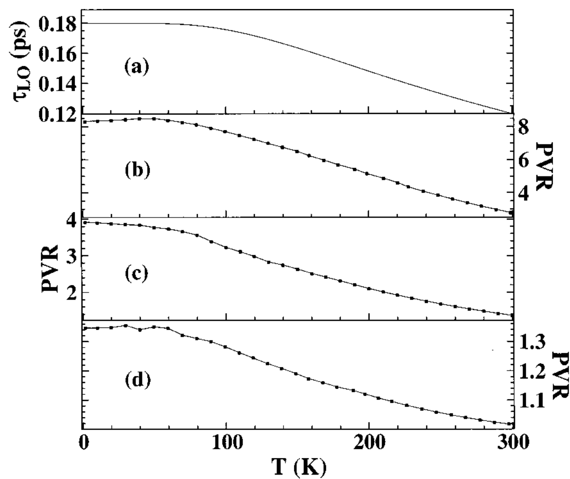

FIG. 6. The effect of the LO phonon interaction on peak-to-valley ratios: (a) the scattering time for an electron in the well with in-plane energy equal to the LO phonon emission threshold (36 meV), (b) the C763 main PVR, (c) the T203 main PVR, (d) the C767 oscillation PVR, for the oscillation at ~1.55 V.

phonon emission, and the second due to absorption. Note that with in-plane electron energies $\geqslant \hbar \omega_{LO}$, emission is a much quicker process: even at room temperature emission is eight times faster. The scattering time τ_{LO} is plotted as a function of temperature in Fig. 6(a), decreasing at a knee around 80 K from a low-temperature value of 0.18 ps. This is much less than the well lifetimes, suggesting a *sequential* process for tunneling through the well at the emission threshold energy. Higher-energy electrons would emit phonons more rapidly, from which we conclude phase coherence through the entire device is not a requirement for observation of the oscillations. This is understood by use of the uncertainty relation, which gives a scattering broadened linewidth $\Gamma \approx \hbar/\tau_{LO} \approx 3.7$ meV; a figure much below the spacer-state separation. So, scattering in the well does little to affect the on-alignment/off-alignment transmission contrast. It does, however, affect the on-resonance/off-resonance PVR, shown for C763 and T203 in Figs. 6(b) and 6(c).

The similarity between Figs. 6(a), 6(b), and 6(c) can be explained using the model of Büttiker.[23] This considers on- and off-resonant transmission through a double barrier in the presence of phase randomization and scattering-induced broadening of the well state. For a wide incident carrier distribution, the peak-to-valley ratio of the on and off-resonant current was shown to vary as $\sim 1/\Gamma$. With a linewidth dominated by scattering-induced broadening, one would, therefore, expect the PVR to be proportional to the scattering time, using the uncertainty relation $1/\Gamma = \tau/\hbar$. Applying that expectation in comparing Figs. 6(a), 6(b), and 6(c) is by no means rigorous, since Büttiker's model was derived for a one-dimensional conductor. Here the situation is complicated by our wide range of in-plane electron energies, and the dependence of the scattering time on those energies. In addition, other scattering mechanisms contribute to the valley current—if not its temperature dependence, and cannot be easily factored out. In lieu of a mathematical comparison, we suggest that the *form* of the curves be compared. The similarity implies the PVR decreases as a result of LO phonon scattering in the well. This is in the most part emission, with the slight upward curve at high temperature in Fig. 6(c) resulting from the absorptive component of Eq. (2). One would expect these conclusions to hold for any RTD which satisfies the conservation requirement for LO phonon emission; namely, one with large in-plane energies (heavy emitter doping) and sparsely occupied wells (thin barriers).

The arguments of Büttiker can be applied to the spacer states, by considering the on-resonance oscillations to result from resonant transmission through the spacer, with electrons incident from a narrow probing well state. "On resonance" then corresponds to alignment of the well state with a spacer state, and "off resonance" corresponds to an off-alignment situation. The peak-to-valley ratio of an oscillation then gives a measure of spacer-state broadening and hence scattering in the spacer. The oscillation PVR is easily defined for C767; the temperature dependence for the oscillation at ~1.55 V is shown in Fig. 6(d). At 1.5 K, the peak position of this oscillation is approximately 80% of the way between the threshold and peak of the main resonance, predicting a tunneling energy $\approx 20\% \times E_{fe} = 0.2 \times 82$ meV ≈ 16 meV. This is sufficiently remote from the Fermi energy to be unaffected by thermal activation of the supply function. Note the spacer density of states has many broad peaks, and is not appropriate for application of Eq. (2). A bulk scattering formula[28] with electron energies $> E_0 = 107$ meV was found to give results much like those of the 2D formula however, so we conclude that the similarity between Figs. 6(a) and 6(d) implies oscillation strengths determined by LO phonon scattering in the spacer, in the most part emission.

IV. MODELING

We have modeled the characteristics of the SCRTD's using a phase-coherent envelope function with a linear voltage profile. Results for one of the devices (C763) are presented here. Airy functions were used to speed computation in the GaAs regions, necessitating a neglect of nonparabolicity. We have ignored charge buildup in the well, which in a rigorous treatment would require a self-consistent Poisson correction to the linear voltage approximation. The screening effect of charge thus modeled would make the well-state energy less sensitive to bias. The correction required to account for this was calculated using the current continuity equation and Poisson's equation to be 0.1 V/ma for C763, extending the resonance by ~0.2 V. Provision for inclusion of such effects was seen to be unnecessary in this discussion.

Beyond flat band bias, the device transmission $T(E_\perp)$ has a single peak at the tunneling energy of the well-state. This has a Lorentzian line shape, allowing a curve fit determination of well-state energy, maximum transmission, and lifetime. These are displayed as a function of bias in Fig. 7. Note that here the lifetime is defined though the uncertainty relation by the coherently modeled Lorentzian linewidth.[17] Since transport through the well is by far the rate limiting step, it can be regarded as the well lifetime.

The spacer standing wave interference has a negligible effect on well-state energy; this is linearly related to applied bias in the linear potential model. The interference affects maximum transmission and lifetime through modulation of

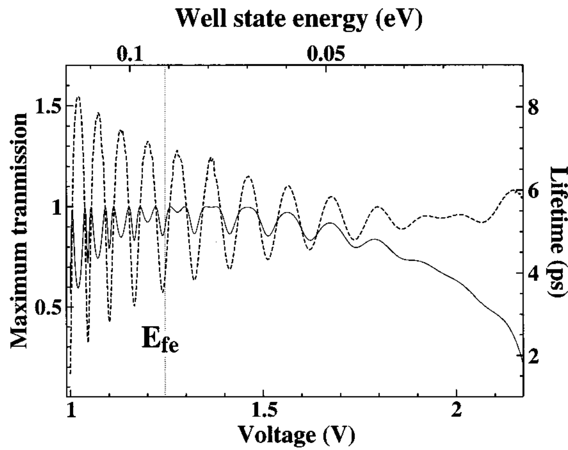

FIG. 7. C763 maximum device transmission (solid) and lifetime (dashed) beyond flat band bias.

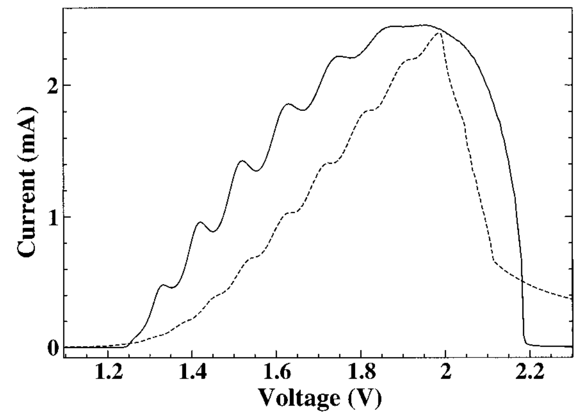

FIG. 8. C763 theoretical (solid) and experimental (dashed) *I-V* curves at 1.5 K.

the spacer density of states, causing bias dependent oscillations. Each dip in lifetime corresponds to a dip in maximum transmission as the well state aligns to a spacer state. This is equivalent to tunnel broadening of the well state—with a broadened Lorentzian linewidth, the *integrated* transmission increases, implying through Eq. (1) an increase in conductance. Peaks in lifetime occur when the well state lies between spacer states. The conductance dips here, so overall we get conductance oscillations of the same period as the lifetime. The lifetime appears to be physically more meaningful than maximum transmission, since it relates directly to conductance through integrated transmission. The maximum transmission oscillates in a rather peculiar manner, *decreasing* when the states align, and seeming to fold over $T=1$ at low bias. The behavior demonstrates that caution is required in describing SCRTD-like structures. Phrases such as ''transmission increases when the states align'' could be wrong, unless it is understood that it is the *integrated* transmission that increases, as a result of tunnel broadening. Note that the sharply oscillating structure of the low bias transmission is unrelated to proximity splitting: the transmission line shape remains Lorentzian here, since electrons beyond flat band are poorly confined to the spacer, possessing a (relative) probability amplitude insufficient for splitting of the well state. The drop in maximum transmission at high bias results from the increasing asymmetry of the double barrier.

The lifetime oscillates like a damped sinusoid about $\tau \approx 5.4$ ps. The damping results from a decreasing above-barrier reflection coefficient, which can be shown using a plane-wave approximation to vary monotonically as

$$R=\left(\frac{\sqrt{m^*/m_e(1+\phi/E)}-1}{\sqrt{m^*/m_e(1+\phi/E)}+1}\right)^2, \tag{3}$$

where $\phi=eV_s+E_{fc}\approx 12.4$ eV is the potential drop into the aluminum. At high bias the reflection is negligible, and the lifetime settles down to the intrinsic double barrier value. This is the value that would normally be used in calculation of device inductance L, for biases in the NDR region. The aluminum reflection should therefore have little effect on calculation of $f_{\max}$ in this device.

The current calculated with Eq. (1) is displayed in Fig. 8, comparing theory and experiment at 1.5 K. The peak heights were matched by increasing the electric-field penetration of the emitter from zero to 18 Å. This increased the peak height at the expense of resonance width (the well state dropped more quickly with bias, causing the device to go off resonance sooner). In spite of this the modeled resonance width is overly large—one would expect it to be narrower than experiment given the neglect of well charge. The neglect of scattering in the well leads to underestimation of valley current, while the neglect of scattering in the spacer leads to an overestimation of oscillation strength. The oscillation spacing, however, agrees fairly well.

Similar attempts at modeling the C767 low-temperature characteristic dramatically underestimated oscillation strength, in spite of the neglect of scattering in the spacer. This may be related to the parabolic band assumption. The aluminum reflection coefficients calculated using flux matching conditions depend on velocities or wave vectors grossly overestimated by the parabolic assumption. Reduced incident velocities give an increased reflection coefficient, so a full nonparabolic model may better predict oscillation strength, as would incorporation of scattering in the spacer. It would nonetheless be difficult to calculate $f_{\max}$ for a device exhibiting such strong oscillations, since the lifetime and inductance could change significantly within the NDR region, according to bias-dependent alignment of the well state and spacer states. Use of the intrinsic double barrier inductance would most likely give an inaccurate result.

Before concluding we mention the possibility of probing the superconducting band gap of an *in situ* deposited collector. This would be possible for indium deposited *in situ* on an InAs spacer with an InAs/AlSb RTD. The indium Fermi energy pins above the conduction band of InAs, so the gap would be accessible for probing with the RTD state.

V. CONCLUSIONS

Thin barrier RTD's with a collector spacer and Schottky collector have potential for increased bandwidth, but are prone to electron reflection from the semiconductor-metal interface of the Schottky collector. With *in situ* deposited metal this causes standing-wave interference in the collector spacer. The resulting quasibound states sweep past the RTD well state with increasing bias, causing oscillations to appear on the rising slope of the RTD *I-V* characteristic. Postreso-

nant oscillations result from a momentum nonconserving probing of the spacer states by the transverse X valley state of the second AlAs barrier.

The voltage dependence of oscillation strength results from two opposingly balanced factors: the emitter supply function and metal reflection coefficient. The temperature dependence of oscillation strength also comes from two opposingly balanced factors: the emitter supply function and scattering within the spacer. A comparison of time scales and temperature-dependent behavior shows this scattering is dominated by interaction with LO phonons, consisting mostly of emission. LO phonon emission by electrons confined to the RTD well causes a related temperature-dependent degradation of the RTD peak-to-valley current ratio.

The number of on-resonance oscillations depends on two parameters: emitter doping level and spacer width. The former determines the resonance width—wider at high temperatures, allowing observation of more oscillations. The latter determines the oscillation spacing through the spacer state separation and voltage scaling. The oscillations move with temperature according to the GaAs band-gap temperature dependence, implying a pinning of the aluminum Fermi energy relative to the GaAs valence-band edge and hence pinning states with valence-band wave functions.

A coherent envelope-function effective-mass model was used to describe low-temperature SCRTD characteristics. The device lifetime was seen to oscillate as a function of bias due to the bias-dependent alignment of spacer states with the well state. While the model was lacking in the use of parabolic bands, neglect of scattering and charge, it is apparent that the lifetime oscillation will cause an oscillation of device inductance L. This could complicate calculation of $f_{\max}$, the maximum speed of operation.

ACKNOWLEDGMENTS

A. J. North thanks the Cambridge Commonwealth Trust for financial support. This work was partially funded by the EPSRC.

*Electronic address: ann1000@cam.ac.uk

[1] E. R. Brown, J. R. Soderstrom, C. D. Parker, L. J. Mahoney, K. M. Molvar, and T. C. McGill, Appl. Phys. Lett. **58**, 2291 (1991).

[2] E. R. Brown, C. D. Parker, and T. C. L. G. Sollner, Appl. Phys. Lett. **54**, 935 (1989).

[3] E. R. Brown, T. C. L. G. Sollner, C. D. Parker, W. D. Goodhue, and C. L. Chen, Appl. Phys. Lett. **55**, 1777 (1989).

[4] J. R. Soderstrom, E. R. Brown, C. D. Parker, L. J. Mahoney, J. Y. Yao, T. G. Andersson, and T. C. Mcgill, Appl. Phys. Lett. **58**, 275 (1991).

[5] Y. Konishi, S. T. Allen, M. Reddy, and M. J. W. Rodwell, Solid-State Electron. **36**, 1673 (1993).

[6] R. P. Smith, S. T. Allen, M. Reddy, S. C. Martin, J. Liu, R. E. Muller, and M. J. Rodwell, IEEE Electron Device Lett. **15**, 295 (1994).

[7] M. V. Weckworth, J. P. A. van der Wagt, and J. S. Harris, J. Vac. Sci. Technol. B **12**, 1303 (1994).

[8] T. Figielski, T. Wosinski, S. A. Vitusevich, A. E. Belyaev, A. Makosa, and W. Dobrowolski, Semicond. Sci. Technol. **12**, 86 (1997).

[9] M. Missous, E. H. Rhoderick, and K. E. Singer, J. Appl. Phys. **59**, 3189 (1986).

[10] I. Zailer, J. E. F. Frost, V. Chabasseur-Molyneux, C. J. B. Ford, and M. Pepper, Semicond. Sci. Technol. **11**, 1235 (1996).

[11] C. E. Timmering, J. M. Lagemaat, C. T. Foxon, and J. J. Harris, Semicond. Sci. Technol. **3**, 1139 (1988).

[12] P. Gavrilovic, J. M. Brown, R. W. Kaliski, N. Y. Holonyak Jr., K. Hess, M. J. Ludowise, W. T. Dietze, and C. R. Lewis, Solid State Commun. **52**, 237 (1984).

[13] R. Tsu and L. Esaki, Appl. Phys. Lett. **22**, 562 (1973).

[14] J. S. Blakemore, J. Appl. Phys. **53**, 520 (1982).

[15] J. Y. Duboz, P. A. Badoz, F. A. Davitava, and E. Rosencher, Phys. Rev. B **40**, 10 607 (1989).

[16] P. Pfeffer and W. Zawadzki, Phys. Rev. B **53**, 12 813 (1996).

[17] P. J. Price, Phys. Rev. B **38**, 1994 (1988).

[18] M. L. Leadbeater, L. Eaves, P. E. Simmonds, G. A. Toombs, F. W. Sheard, P. A. Claxton, G. Hill, and M. A. Pate, Solid-State Electron. **31**, 707 (1988).

[19] M. L. Leadbeater, E. S. Alves, L. Eaves, M. Henini, O. H. Hughes, A. Celeste, J. C. Portal, G. Hill, and M. A. Pate, Phys. Rev. B **39**, 3438 (1989).

[20] T. J. Foster, M. L. Leadbeater, L. Eaves, M. Henini, O. H. Hughes, C. A. Payling, F. W. Sheard, P. E. Simmonds, G. A. Toombs, G. Hill, and M. A. Pate, Phys. Rev. B **39**, 6205 (1989).

[21] T. W. Hickmott, Phys. Rev. B **32**, 6531 (1985).

[22] B. fen Zhu and K. Huang, Phys. Rev. B **48**, 4575 (1993).

[23] M. Büttiker, in *Resonant Tunneling in Semiconductors*, edited by L. L. Chang *et al.* (Plenum Press, New York, 1991), p. 213.

[24] 247 meV for the transverse X valley of a 20-Å AlAs barrier, calculated relative to the GaAs Γ conduction band.

[25] R. Ferreira and G. Bastard, Phys. Rev. B **40**, 1074 (1989).

[26] B. A. Mason and S. Das Sarma, Phys. Rev. B **35**, 3890 (1987).

[27] There is a misprint in the quantum-well definition of $f(q)$ in the previous reference: the isolated q factor should read qa.

[28] K. Seeger, in *Semiconductor Physics: An Introduction*, edited by Editor(s), Springer Series in Physics Vol. 40 (Springer-Verlag, Berlin, 1982), p. 199.